A Statistical Analysis of Copper Bottom Coverage of High-Aspect-Ratio Features Using Ionized Physical Vapor Deposition

T. G. Snodgrass, *Student Member, IEEE* and J. L. Shohet, *Fellow, IEEE*

***Abstract*—Ionized physical vapor deposition (IPVD) is a new method for depositing metal into high-aspect-ratio features used as interconnects in microelectronic fabrication. It is similar to sputtering except that a portion of the metal flux to the substrate is ionized. We show how a high ionized-metal-flux fraction (IMFF) at the deposition location improves the bottom coverage of deposited metal films. To measure IMFF, a tool was developed, that biased the front surface of a microbalance crystal directly so as to repel ions. Cu IMFFs to the substrate of greater than 90% along with deposition rates of 1000 Å/ min can be achieved. A statistical model for both IMFF and total metal flux as a function of four control variables: chamber height, Ar pressure, ionizer power, and sputter power was developed.**

***Index Terms*—Bottom coverage, copper, deposition, ionized physical vapor deposition, plasma, sputtering, statistics.**

I. Introduction

SEMICONDUCTOR manufacturers continually face scientific and manufacturing challenges as the critical dimensions of the patterned features on silicon wafers decrease. The formation of the metal wiring for interconnection of the various circuit elements is an important step in the manufacture of integrated circuits (ICs). The metallization steps have traditionally been accomplished by physical vapor deposition (PVD) and chemical vapor deposition (CVD).

A critical concern facing the IC industry is the need to metallize high aspect ratio structures, i.e., structures with a vertical dimension greater than their lateral dimension. Ionized physical vapor deposition (IPVD) is a new PVD method that addresses the need to metallize high aspect ratio features. This paper examines the optimization of the copper IPVD process [1] for use in such high aspect ratio features.

A. Problems Faced in the Metallization of High Aspect Ratio Features

Metal deposition for contacts, vias, and trenches is typically a two-step process: 1) depositing a conformal liner, and 2) filling the feature with high-conductivity metal. Thus, prior to filling a feature with high-conductivity metal, the surface of the feature must be conformally coated with 100 to 500 Å of liner metal. After the conformal liner has been deposited, the feature is then filled with a high conductivity metal. Typical features have a height on the order of 1 μm. Since filling requires films 100 times thicker than those needed for producing conformal liners, the two processes face different problems and need to be investigated separately.

B. Filling

As the aspect ratio of features increases, traditional sputtering becomes ineffective to fill these features. The isotropic trajectories of the depositing metal atoms cause metal to be deposited faster on the upper surface of the wafer and around the upper edges of a hole than into the bottom of the hole. As the aspect ratio is increased, the nonuniform deposition can become so serious that the top of the hole pinches off before the hole is filled and thus leaves a buried void.

Typical materials for filling features are W, Al, and Cu. The resistivity of Al is less than W and the resistivity of Cu is even less than Al. For this reason, it is likely that less and less W will be used in interconnects and the metallizing step will eventually move away from Al and entirely to Cu. It is unlikely that W will be used for fill metal in high-aspect-ratio features, because it is likely to be phased out before the aspect ratio will be too high for conventional sputtering methods.

C. Lining

There is no fear of closing off high-aspect-ratio features when lining, because the films are designed to be much thinner than the minimum feature width. Typical lining materials Ti, TiN, Ta, TaNi, W, and WNi, have a much higher resistivity than those of many fill materials. It is therefore desirable to keep the liner as thin as possible so that the contact or via can be filled primarily with a high conductivity metal such as Cu.

The goals of a good high-aspect-ratio feature lining process are uniform sidewalls and bottom coverage. For contacts, it is desirable to have thicker bottom coverage to give extra protection to the underlying Si substrate. In a similar fashion to *filling* high-aspect-ratio features, traditional sputtering has difficulties *lining* high-aspect-ratio features. The process tends to deposit the metal largely around the upper sidewalls of a hole but deposits onto the bottom and lower sidewalls at a much slower rate.

We show here how it is possible to optimize the deposition rate while still retaining a high fraction of ionized particles in the plasma, which, we believe, will make the process most effective in metallization of high-aspect-ratio features. The two conditions (high deposition rate and high ionization fraction)

Manuscript received March 20, 2001. This work was supported in part by the National Science Foundation under Grant ECS-8721545.

The authors are with the Center for Plasma-Aided Manufacturing and Department of Electrical and Computer Engineering, University of Wisconsin-Madison, Madison, WI 53706 USA.

Publisher Item Identifier S 0894-6507(02)01033-3.

0894–6507/02$17.00 © 2002 IEEE

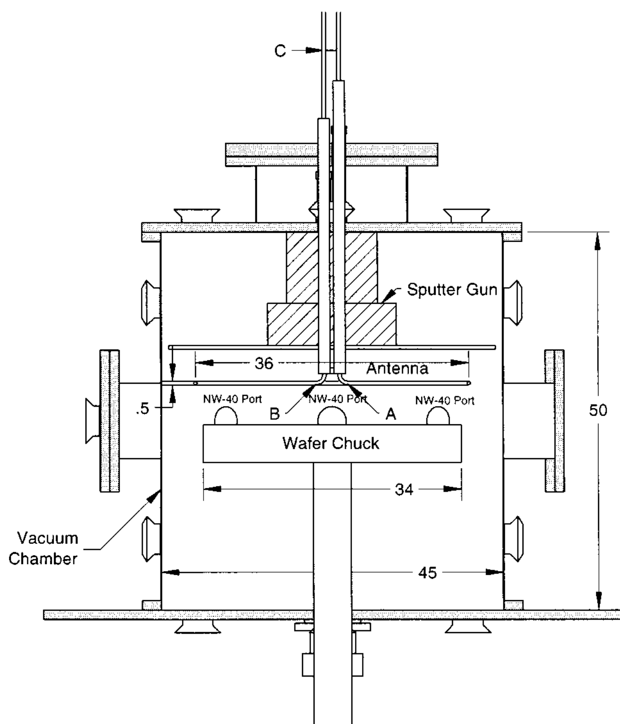

Fig. 1. Cross-sectional schematic diagram of vacuum chamber showing location of main components. All dimensions in cm.

often require opposite operating conditions. For example, a high fraction of ionized particles will result when the neutral particles spend the longest time possible between the sputtering target and the substrate. To obtain a high deposition rate, on the other hand, the sputtering target should be placed as close as possible to the substrate. Similar opposing conditions also appear in the casse of gas fill pressure, as well as sputter and ionizer power levels. Furthermore, even after optimizing these two quantities (ionization fraction and deposition rate) we must further examine these conditions on the effectiveness of bottom coverage of the deposited metal.

It must be noted that in practice the aspect ratios that are utilized in this work are often higher and the liner coverage on the sidewalls becomes more of a critical issue than bottom coverage. Although our experimental work does not consider these higher aspect ratios, the optimization methods utilized here can be applied to liner coverage at higher aspect ratio conditions.

II. Experimental Apparatus

A. Vacuum Chamber

An aluminum cylinder, 45 cm in diameter by 50 cm tall, defines the main volume of the vacuum chamber as shown in Fig. 1. The cylinder rests on an aluminum base plate that has a number of ports. It is possible to flow up to three gases into the vacuum chamber at one time, but for nearly all experiments, Ar was the only gas used and its flow rate was set to 25 sccm.

B. Other System Components

The temperature of the chamber is controlled with heat tape. When there is plasma in the vacuum chamber, the heat tape plus the additional power from the plasma source allows the chamber to regulated to 100 °C for all experiments. A water-cooled wafer chuck, large enough for a 300-mm wafer, is installed along the centerline of the vacuum chamber through a quick connect in the base plate of the chamber.

A commercial 5-kW 15-cm diameter magnetron sputter gun is installed through a port in the center of the top lid of the chamber. The location of the gun target surface can be adjusted between 7.5 and 28 cm above the wafer chuck. A copper water-cooled target was used for all experiments. An aluminum annular disk was attached to the sputter gun so that the target protruded through the ID of the disk and was flush with the disk's front surface. The disk served as an artificial vacuum chamber wall so we were able to measure the effects of a variable chamber height on process conditions. When the target surface was not flush with the top of the vacuum chamber, this artificial "chamber wall" defined the upper edge of the process chamber. Hence, as in a production system, plasma and sputtered metal cannot extend above the plane of the sputtering target.

C. Ionizer Antenna

In order to ionize the metal vapor as it drifts from the sputtering target to the wafer chuck, an auxiliary plasma (in addition to that produced by the sputter gun) was created between the sputter target and the wafer chuck. The plasma must be dense and uniform over the sputtering plane. Several methods for producing the auxiliary plasma have been implemented. They are: electron cyclotron resonance [1], a 13.56-MHz internal antenna inductively coupled plasma [2] and a 13.56-MHz external antenna inductively coupled plasma with an internal Faraday shield [3].

We used a single turn antenna inside the vacuum chamber fed with 13.56-MHz r.f. power. Placing the antenna inside the vacuum chamber, where it will be in intimate contact with the plasma, is unique to IPVD systems. By comparison, inductively coupled plasma etchers have an antenna external to the vacuum chamber, and the electric fields are coupled through a quartz window. An internal antenna is preferred for IPVD because if the antenna were placed outside a dielectric wall [3], sputtered metal would quickly coat the inside of the wall and shield out fields produced by the antenna.

The plasma it produces can sputter the antenna itself. This is especially true if dc current is not allowed to flow between the antenna and ground by blocking capacitors. The rectifying effect of the plasma tends to create a self bias on the antenna much like the self bias which occurs during RF sputtering of a nonconductive target, or the self bias that often appears on a substrate placed in a plasma under RF excitation. Copper was chosen for the antenna so that sputtered antenna material would contribute to the copper films being deposited, rather than contaminate them. The antenna was always located 5 cm above the wafer chuck.

III. Experimental Results and Analysis

This section begins with a description of how the copper metal vapor can become ionized to a large fraction and retains reasonable deposition rates. We discuss the maximization of the

total metal flux (TMF) for given values of the ionized metal flux fraction (IMFF) followed by a discussion of optimization of bottom coverage.

A. Maximization of TMF as a Function of IMFF

It has been shown in the literature that IPVD systems can achieve fairly high IMFFs. However, a general trend observed in most IPVD experiments is that when the IMFF is increased, the TMF decreases. It is therefore important when trying to achieve a high IMFF to ensure that the TMF is not so low that the process will not be usable.

A special quartz crystal microbalance [4] was developed to differentiate between depositing ions and neutrals by biasing the front surface of the crystal to repel ions. Furthermore, we chose to use the width at the top of the SiO_2 of the wafer as the width and the distance from the top of the SiO_2 to the bottom center of the trench as the height of the trench.

The measurement used to quantify metal film coverage was bottom coverage. Bottom coverage is the ratio of the metal film thickness at the bottom center of the feature to the metal film thickness on the main surface of the wafer. The aspect ratio and bottom coverage can clearly be seen in Fig. 2.

To examine the problem, we will utilize a statistical experimental design. Four input factors will be used. They are: 1) chamber height (h); 2) Ar pressure (p); 3) ionizer power (P_I); and 4) sputter power (P_S). We will use these to maximize two output variables, IMFF and TMF. IMFF and TMF are measured at the center of the substrate with the modified quartz crystal microbalance. We then develop a mechanistic model to show the relationships and show that the maximum TMF always decreases as the IMFF increases. We also show that it is possible to approach a TMF of 1000 $\text{Å}/\min$ with an IMFF of greater than 90%.

The chamber height in the system, i.e., the distance between sputter target and substrate, as described in Section II, was varied between 10 and 26 cm. Through initial experiments, we determined that useful background-gas pressures were from 10 to 90 mtorr. The maximum ionizer power was 2 kW. The maximum sputter power was also 2 kW.

Measurements of the TMF and IMFF were made measured using a $3 \times 3 \times 3 \times 4$ level full factorial experimental design consisting of three chamber heights, three Ar pressures, three ionizer powers, and four sputter powers. Table I shows the levels that were used for each variable.

We develop a mechanistic model for TMF to fit the observed data using the following reasoning. First, TMF should be proportional to sputter power, since sputter rate is approximately proportional to sputter power. Second, TMF should decrease exponentially with both chamber height and Ar pressure, since the probability that a Cu atom will make a momentum-transfer collision with an Ar atom increases exponentially with Ar gas pressure (p) and chamber height (h). We include cross terms to allow additional freedom to model other effects, such as rarefaction of the background gas that occurs as a function of both the sputter power and ionizer power, which would certainly affect

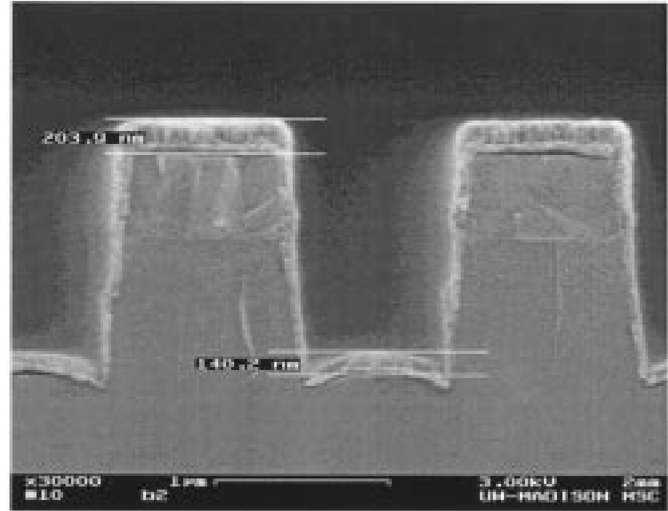

Fig. 2. SEM cross-sectional image of trench covered by a thin copper film. Cross-hairs show how the bottom coverage is measured.

TABLE I
INPUT VARIABLE VALUES

Input Variable	Low Value	Mid Value	High Value
Chamber Height (cm)	10	18	26
Ar Pressure (mtorr)	30	60	90
Ionizer Power (kW)	0	1	2
Sputter Power (kW)	0.5	1	2

the TMF. From these arguments, the form of the mechanistic model is as follows:

$$\begin{aligned}\mathrm{TMF} = P_S \exp\Big(& b_0 + b_1 h + b_2 p + b_3 P_I + b_4 P_S + b_5 hp \\ & + b_6 hP_I + b_7 hP_S + b_8 pP_I + b_9 pP_S \\ & + b_{10} P_S P_I + b_{11} hpP_I + b_{12} hpP_S \\ & + b_{13} hP_I P_S + b_{14} pP_I P_S + b_{15} hpP_I P_S \Big)\end{aligned} \quad (1)$$

where h is the chamber height, p is the pressure, P_S is the sputter power, and P_I is the ionizer power and the coefficients b are the model's fitting parameters. Since (1) is nonlinear in the fitting parameters $b_0, \ldots b_{15}$, nonlinear regression was used to estimate the fitting parameters.

Fig. 3 shows an example of the measured TMF data along with a plot of the mechanistic model, (1) as sputter power and ionizer power are varied, for a fixed chamber height and pressure. The symbols • show the measured data and the mesh curve is a plot of the mechanistic model.

We briefly discuss the dependence of TMF on each of the four input variables. This can be seen by examining Fig. 4 that presents the results of the nonlinear regression. The dashed lines are the 90% confidence limits for the model. Fig. 4 shows, as expected, that an increase in sputter power and ionizer power

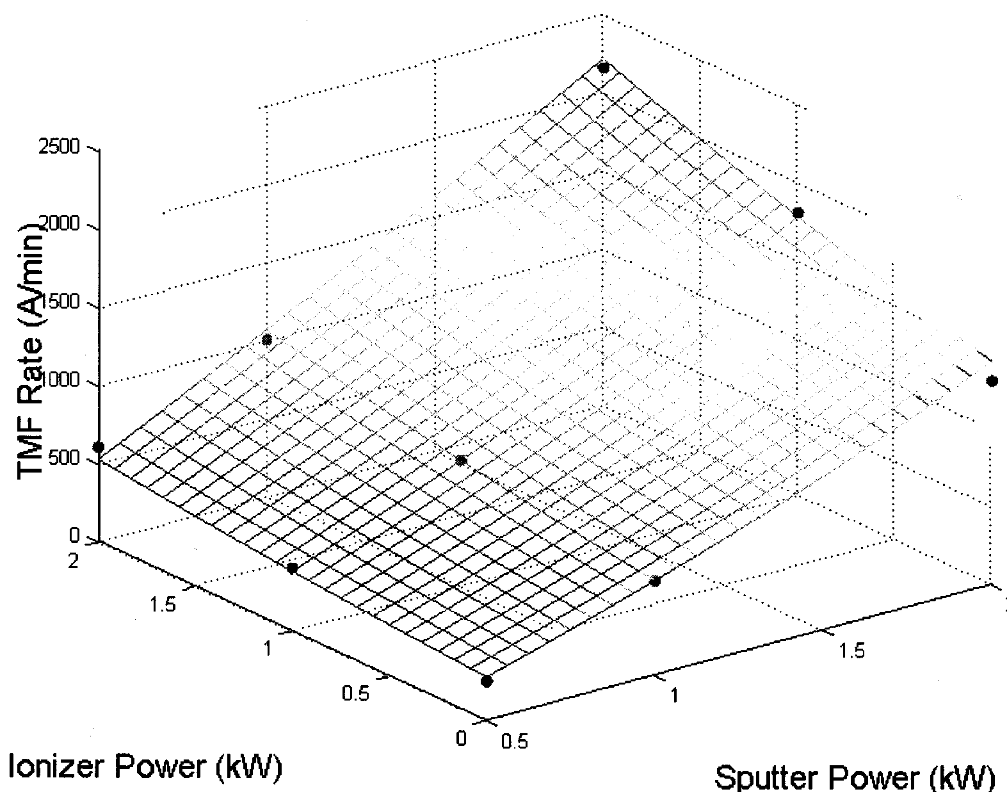

Fig. 3. Nonlinear regression model for TMF shown in comparison to experimental data points.

results in an almost linear increase in TMF. The latter dependence is most likely due to rarefaction of the Ar gas as the ionizer heats it. Rossnagel [5] has shown significant rarefaction of the background gas by heating the gas with the ionizer. Rarefaction of the Ar gas by heating is similar to reducing the Ar pressure, which as we can also see in Fig. 4, increases TMF. TMF also decreases with chamber height. The data show that over the experimental range, TMF is more sensitive to changes in chamber height than to changes in pressure. Concurrent to measuring TMF, IMFF was measured. Fig. 5 shows IMFF as a function of the four input variables, displayed in the same format as for TMF. Similarly to TMF, a mechanistic model was developed for IMFF. The nonlinear mechanistic model for the data, with c's as fitting parameters, is

$$\mathrm{IMFF} = 1 - \exp(P_I p(h - c_0)(c_1 + c_2(h - c_0) + c_3 p + c_4 P_I + c_5 P_S)). \quad (2)$$

The basis for this model is as follows: 1) IMFF should always be between 0 and 1. 2) IMFF should be zero when ionizer power (P_I) or Ar pressure (p) are zero. 3) Since the *neutral* metal flux decreases exponentially to 0 with P_I, p, and h increasing, IMFF will approach 1 as these input variables increase. A linear factor in h, p, P_I, and P_S was added to the exponent to allow additional freedom for regression and allow for the capturing of higher order effects.

Fig. 5 shows that IMFF falls monotonically as the sputter power is increased. In particular, for constant ionizer power, only a finite number of ionizing collisions can occur per unit time. By increasing the Cu atom density with increasing sputter power, the number of ionizing collisions per unit time remains roughly constant, and therefore the IMFF is reduced. Fig. 5 shows, as expected, when ionizer power, Ar pressure or chamber pressure are increased, IMFF increases. The IMFF drops dramatically as the chamber height is reduced to 10 cm, indicating that it is very difficult to ionize Cu vapor in systems with a very short distance between sputter target and substrate. Now that we know how TMF and IMFF vary as a function of the input variables, we are prepared to maximize TMF for a given value of IMFF.

We examine this aspect of the problem by computing surfaces of constant TMF and IMFF as a function of the input variables and examine where they may intersect. Fig. 6 shows the intersection of the surfaces for an IMFF of 60% and a deposition rate of 800 Å/min for a chamber height of 18 cm. The values of ionizer power, sputter power and pressure at the intersection of the two surfaces can be read directly off the Figure. If the surfaces do not intersect, the two desired values of IMFF and TMF cannot be achieved. Thus, this method allows us to set the desired deposition rate and IMFF and find, for a given chamber height, the locus of the plasma parameters at the intersection of the two surfaces that will allow these conditions to occur simultaneously. As expected, the maximum ionizer power (2 kW) was always required to achieve the maximum TMF for given values of IMFF. In fact, increasing the ionizer power always increases IMFF without decreasing TMF. This means, for example, if ionizer power is increased, the pressure or height can be reduced and still maintain the same IMFF. However, increasing the ionizer power does not reduce TMF (it increases it), but lowering the pressure or height increased TMF.

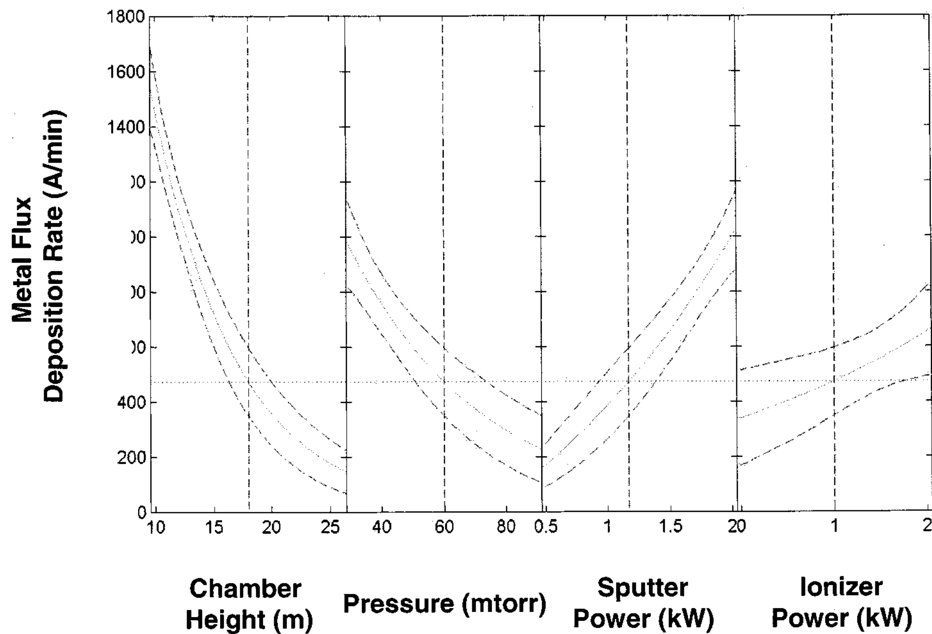

Fig. 4. Nonlinear regression model for TMF as a function of the four input variables. The dashed lines are the 90% confidence limits.

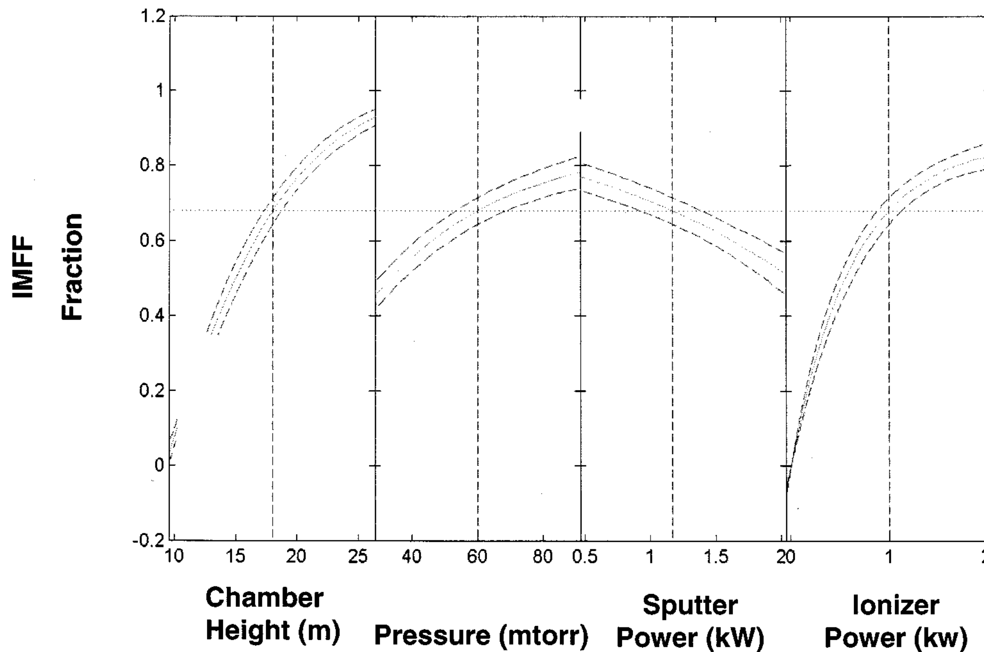

Fig. 5. Nonlinear regression model for IMFF as a function of the four input variables. The dashed lines are the 90% confidence limits.

B. Bottom Coverage

IPVD has been shown to improve metal fill and coverage properties [6]; but no experimental measurements have been published which show a direct relationship between IMFF and metal fill or coverage properties. In this section, we show the relationship between IMFF and bottom coverage. We develop a bottom coverage estimate for both trenches and vias and then compare this with experimental measurements.

Bottom coverage should increase as the IMFF increases due to the fact that the ion flux is oriented nearly perpendicular to the substrate. This occurs because the plasma potential accelerates ions toward the substrate with an energy of approximately 10 eV as compared to the ion thermal energy, which is approximately 0.03 eV. We assume, on the other hand, that the *neutral* flux arrives at the substrate plane with an isotropic velocity distribution. Hence, if an ion arrives at the plane of a trench or via opening, we assume that its probability of reaching the bottom of the trench is one. To verify this, we estimate the mean free path for ion-neutral collisions, which is the dominant momentum-transfer collision mechanism for ions in the plasma sheath and compare this to the sheath thickness plus the trench

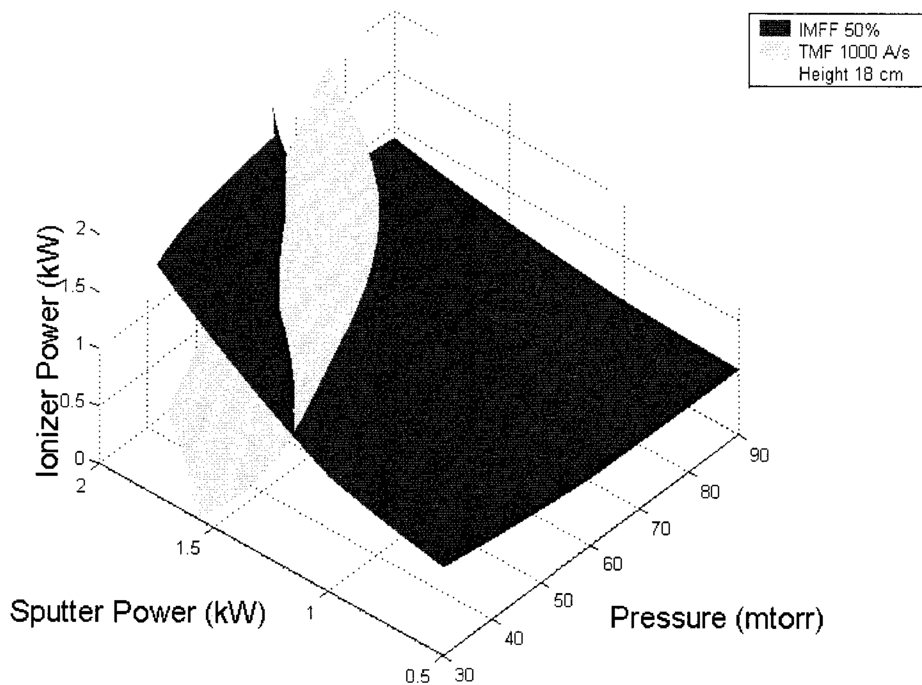

Fig. 6. The intersection of TMF = constant and IMFF = constant surfaces, showing the ranges for the input variables that will produce these conditions concurrently.

or via depth that is the distance ions must travel without being deflected. The mean free path for collisions between metal ions and the background gas λ_i is

$$\lambda_i = \frac{1}{n_g \sigma_m} \tag{3}$$

where n_g is the density of the inert gas and σ_m is the collision cross section for momentum transfer for the ion with the gas. To estimate a minimum value for the mean free path, we find that the gas density at the maximum chamber pressure of 90 mtorr and room temperature is 3×10^{15} cm^{-3}. Grapperhaus *et al.* [6] give the cross section for momentum transfer of Cu on Ar as 20 Å^2. Thus, the mean free path for the ions is 1700 μm. Lieberman and Lichtenbergn [7] give the sheath thickness as a few λ_{Debye} and give the following formula for λ_{Debye} in centimeters:

$$\lambda_{\text{Debye}} = 740\sqrt{\frac{T_e}{n_p}} \tag{4}$$

where T_e is the electron temperature in eV and n_p the plasma density in cm^{-3}. Using a typical electron temperature T_e = 3 eV and plasma density $n_p = 3 \times 10^{12}$, we find $\lambda_{\text{Debye}} = 7.4$ μm or 4 $\lambda_{\text{Debye}} = 30$ μm. A comparison of these numbers with a typical trench or via depth of 1 μm (see Table II) indicates that it is unlikely that ions undergo collisions in the plasma sheath or trench/via even with a high chamber pressure of 90 mtorr.

In estimating bottom coverage, we assume that the sticking coefficient for the metal vapor is approximately one for both the ions and neutrals and that the resputtering rate is zero for both metal and inert gas ions and neutrals. Then, the fraction of neutrals that reach the bottom of a trench can be predicted using a cylindrical-coordinate system centered at the point of deposition with its cylindrical axis running parallel to the trench (see Fig. 7).

TABLE II
COMPARISON OF DISTANCES TO DETERMINE LIKELIHOOD OF IONS BEING DEFLECTED BEFORE DEPOSITION

	Expression	Typical Value (Microns)
Mean Free Path for Momentum Transfer	$1/(n_g\sigma_m)$	1700
Sheath Thickness	$4\lambda_{\text{Debye}}$	30
Typical Trench or Via Depth	NA	1

A point on the upper surface of the substrate would expect metal flux equally from all angles θ between $-\pi/2$ and $\pi/2$. The point at the bottom center of the trench, however, will only receive flux equally for θ between $-\theta_0$ and θ_0. Therefore, the ratio of the flux on the bottom of the trench to flux on the main surface is $2\theta_0/\pi$. From the figure we see that $\theta_0 = \tan^{-1}(W/2H)$. The aspect ratio is defined as $\text{AR} = H/W$. Hence, the fraction of neutrals that reach the bottom of the trench is

$$\frac{2\tan^{-1}\left(\frac{1}{2\text{AR}}\right)}{\pi}. \tag{5}$$

The bottom coverage for trenches (BC_T) expressed in (6) below is the fraction of the metal flux that is ionized plus the fraction of the metal that is not ionized times the probability that a neutral reaches the bottom of the trench. This may be expressed as

$$\text{BC}_T = \text{IMFF} + (1 - \text{IMFF})\frac{2\tan^{-1}\left(\frac{1}{2\text{AR}}\right)}{\pi}. \tag{6}$$

The bottom coverage for vias can be found by using a similar development in spherical coordinates. A point on the main surface

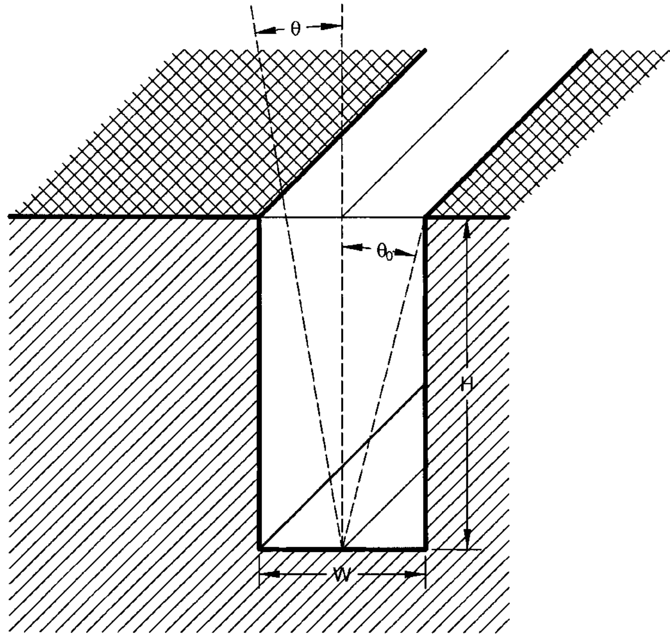

Fig. 7. Cross section of a trench, showing the various quantities used in developing a bottom coverage estimate.

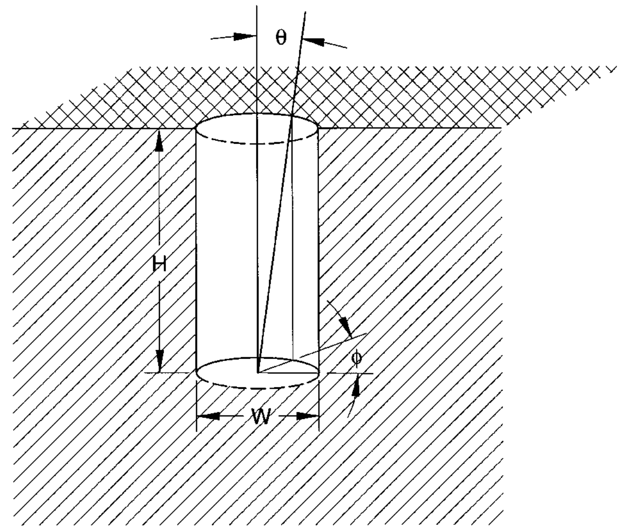

Fig. 8. Cross section of a via, showing the various quantities used in developing a bottom coverage estimate.

of the substrate should receive neutral flux from a solid angle of 2π. The point at the bottom center of a via should receive flux from the solid angle described by the following integral (see Fig. 8)

$$\int_0^{2\pi}\int_0^{\theta_0}\sin(\theta)d\theta d\phi. \tag{7}$$

Evaluating the integral and following a procedure similar to the one we used to find bottom coverage for trenches, we find that the bottom coverage for vias (BC_v) is

$$\mathrm{BC}_V = \mathrm{IMFF} + (1-\mathrm{IMFF})\left(1-\frac{2\mathrm{AR}}{((2\mathrm{AR})^2+1)^{1/2}}\right). \tag{8}$$

Equations (6) and (8) show that bottom coverage depends only on the aspect ratio and not on the absolute dimensions of the trench. We expect these equations to hold over a wide range of via and trench sizes. Note that if deposition continues beyond a very thin film, the aspect ratio of the trench or via will change, and hence, the bottom coverage will change as the film thickness changes.

For the experimental measurements, samples were prepared as presented in Section III with aspect ratios of 1.2 for trenches and 2.0 for vias. Both features had openings 1.1 μm wide.

Figs. 9 and 10 show the results of depositions onto substrates with 1.2 aspect ratio trenches and 2.0 aspect ratio vias, respectively as a function of IMFF. One can see a clear increase in bottom coverage as the IMFF increases. The data agree well with our theoretical predictions. A linear fit to the data and 90% confidence intervals for the expected value of bottom coverage has also been plotted with the measured data. Linear fits to the data are:

$$\mathrm{BC}_T = 0.51\,\mathrm{IMFF} + 0.46;\ \text{for } \mathrm{AR} = 1.2 \tag{9}$$

$$\mathrm{BC}_V = 0.68\,\mathrm{IMFF} + 0.10;\ \text{for } \mathrm{AR} = 2.0. \tag{10}$$

In both figures, the linear fits lie below the theoretical model at a value of $\mathrm{IMFF} = 1.0$. This is likely because the ion flux is not oriented perfectly perpendicular to the substrate and some of the ions are lost to the walls of the trench or via. In these experiments, the wafer chuck was not biased; hence the ions are relying on the natural difference between the plasma potential and ground to accelerate them perpendicular to the substrate. It should be possible to bias the wafer chuck to an average potential well below the plasma potential, thus increasing the perpendicular acceleration of the ions toward the substrate. This would increase the anisotropy of the ions and make the bottom coverage closer to the predicted bottom coverage for IMFF near 1.0. For IMFF near 0.0, the bottom coverage, for both trenches and vias, is greater than that predicted. This is probably due to the fact that the neutrals are not perfectly isotropic at the entrance to the trench or via and are more likely to get to the bottom than previously assumed.

In order to include both of these effects, an improved mechanistic model was developed, as shown in the following:

$$\begin{aligned}\mathrm{BC}_T =& \kappa\,\mathrm{IMFF} + (1-\nu)(1-\mathrm{IMFF})\frac{2\tan^{-1}\left(\frac{1}{2\mathrm{AR}}\right)}{\pi} \\ &+ \nu(1-\mathrm{IMFF}) \\ =& \kappa\,\mathrm{IMFF} + (1-\mathrm{IMFF}) \\ &\times\left((1-\nu)\frac{2\tan^{-1}\left(\frac{1}{2\mathrm{AR}}\right)}{\pi}+\nu\right)\end{aligned} \tag{11}$$

$$\begin{aligned}\mathrm{BC}_\nu =& \kappa\,\mathrm{IMFF} + (1-\nu)(1-\mathrm{IMFF}) \\ &\times\left(1-\frac{2\mathrm{AR}}{((2\mathrm{AR})^2+1)^{1/2}}\right) \\ &+ \nu(1-\mathrm{IMFF})\kappa\,\mathrm{IMFF} + (1-\mathrm{IMFF}) \\ &\times\left((1-\nu)\left(1-\frac{2\mathrm{AR}}{((2\mathrm{AR})^2+1)^{1/2}}\right)+\nu\right).\end{aligned} \tag{12}$$

Note that (11) and (12) remain linear in IMFF, just as (6), (8)–(10). κ is the fraction of the ions that make it to the bottom

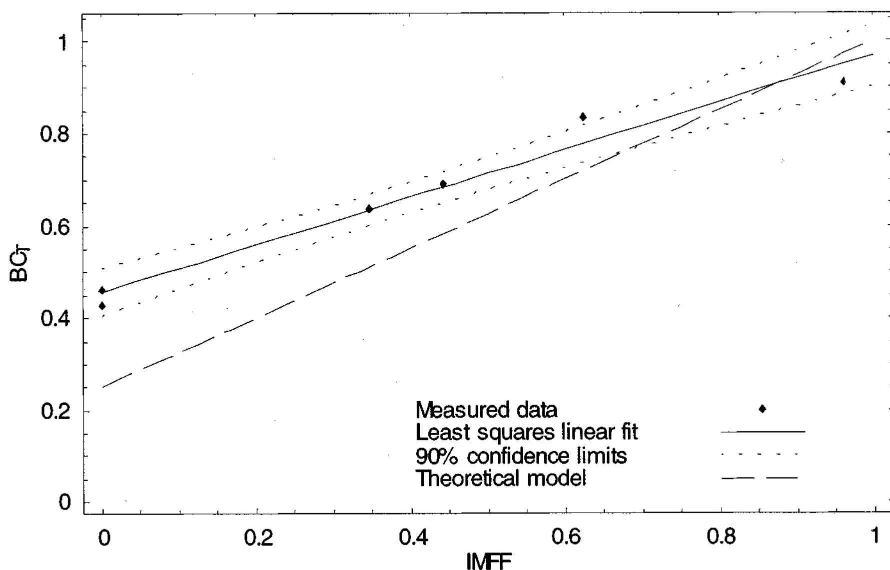

Fig. 9. Bottom coverage of 1.2 aspect ratio trenches as a function of IMFF. Diamonds are experimental measurements. The thin line is the simplified theoretical model given by (8). The thick line is a linear least squares fit to the data given by the equation $\mathrm{BC}_T(\mathrm{AR}=1.2)=0.51\,\mathrm{IMFF}+0.46$ which is also used in the final theoretical model governed by (9).

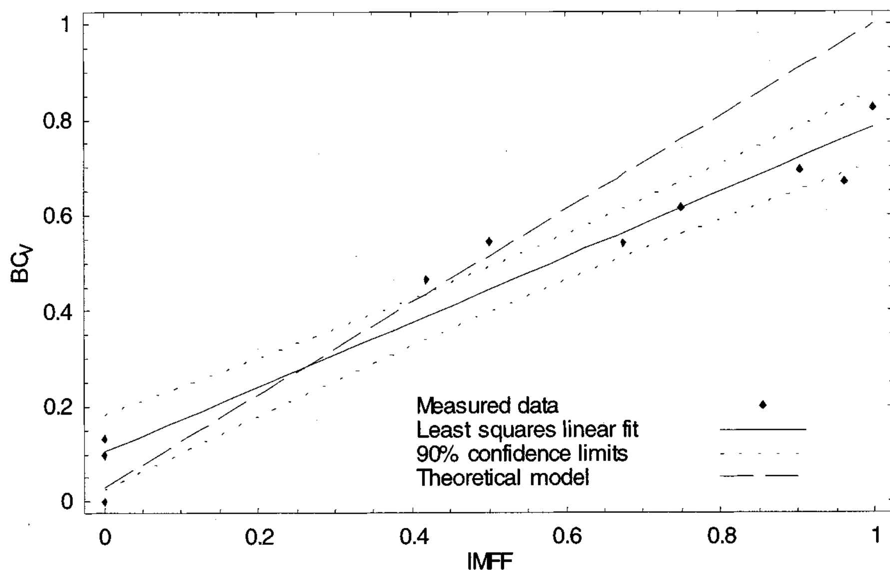

Fig. 10. Bottom coverage of 2.0 aspect ratio vias. Diamonds are experimental measurements. The dashed line is the simplified theoretical prediction given by (9). The solid line is the linear fit to the data given by equation $\mathrm{BC}_V=0.68\,\mathrm{IMFF}+0.10$ which is also used in the final theoretical model governed by (10). The dotted lines are the upper and lower 90% confidence limits for the expected value of BC_V.

of the trench or via. κ can have a value between 0 and 1. The parameter ν is the fraction of the neutrals that are anisotropic, and is between 0 and 1, where 0 is a perfectly isotropic distribution. We assume that all anisotropic neutrals entering the trench or via reach the bottom and are not affected by the aspect ratio as the isotropic neutrals are. Solving (9)–(12) for the values of κ and ν to match the linear fit for 1.2 aspect ratio trenches and 2.0 aspect ratio vias give the values shown in Table III below.

Note that κ, the fraction of ions that reach the bottom of the trench or via, is large, near unity, but it is not as large for the 2.0 aspect ratio via compared to the 1.2 aspect ratio trench. ν, the fraction of neutrals that are anisotropic, is small near 0.

TABLE III
VALUES OF κ AND ν

	κ	ν
AR=1.2 Trench	0.97	0.16
AR=2.0 Via	0.78	0.07

IV. Summary and Conclusion

The work presented here shown that the most effective bottom coverage for copper deposition takes place with the highest fraction of copper atoms ionized. We are able to determine the values of the external input control variables to

allows the simultaneous optimization of both ionized metal flux fraction and total metal flux deposition rate even though the factors that influence these quantities do so in opposition. This permits us to operate IPVD systems at the highest deposition rate possible while maintaining the most effective bottom coverage. Without the use of an effective statistical experimental design, it was not possible to obtain such results and the mechanistic model developed using this method can be easily applied to other processing systems.

In particular, in order to investigate liner thickness midway up the feature sidewall instead of bottom coverage, the same methods can be used with measurements of liner thickness measured as a function of the key control variables used in this work.

ACKNOWLEDGMENT

Grateful thanks are due to A. E. Wendt and Z. H. Lu for their assistance with the experimental portion of this work.

REFERENCES

[1] W. M. Holber, J. S. Logan, H. J. Grabarz, J. T. C. Yeh, J. B. O. Caughman, A. Sugerman, and F. E. Turene, "Copper deposition by electron cyclotron resonance plasma," *J. Vac. Sci. Technol. A*, vol. 11, pp. 2903–2910, 1993.

[2] S. M. Rossnagel and J. Hopwood, "Magnetron sputter deposition with high levels of metal ionization," *Appl. Phys. Lett.*, vol. 63, pp. 3285–3287, 1993.

[3] M. Dickson, G. Zhong, and J. Hopwood, "Radial uniformity of an external-coil ionized physical vapor deposition source," *J. Vac. Sci. Technol. B*, vol. 16, pp. 523–531, 1998.

[4] T. G. Snodgrass, J. H. Booske, W. Wang, A. E. Wendt, and J. L. Shohet, "Gridless ionized metal flux fraction measurement tool for use in ionized physical vapor deposition studies," *Rev. Sci. Instr.*, vol. 70, pp. 1525–1529, 1999.

[5] S. M. Rossnagel, "Directional and ionized physical vapor deposition for microelectronics applications," *J. Vac. Sci., Technol. B*, vol. 16, pp. 2585–2608, 1998.

[6] M. J. Grapperhaus, Z. Krivokapic, and M. J. Kushner, "Design issues in ionized metal physical vapor deposition of copper," *J. Appl. Phys.*, vol. 83, pp. 35–43, 1998.

[7] *Principles of Plasma Discharges and Materials Processing*, M. A. Lieberman and A. J. Lichtenberg, Eds., Wiley Interscience, New York, 1994.

T. G. Snodgrass (S'96) received the B.S. degree in physics and mathematics in 1991, the M.S. degree in mathematics in 1994 from the University of Nebraska, Lincoln, and the Ph.D. degree in electrical and computer engineering from the University of Wisconsin-Madison, in 1999.

From 1990 to 1991, he had internships at the University of Colorado, Boulder, Argonne National Laboratories, and Sandia National Laboratories and is currently employed at Cypress Semiconductor, Minneapolis.

J. L. Shohet (S'56–M'62–SM'72–F'78) received the Ph.D. degree in electrical engineering from Carnegie Mellon University, Pittsburgh, PA, in 1961.

He served on the faculty of The Johns Hopkins University before joining the University of Wisconsin faculty in 1966 and was appointed Professor of Electrical and Computer Engineering in 1971. He is the Founding Director of the Torsatron/Stellarator Laboratory, a major U.S. Department of Energy fusion research facility, and the Founding Director of the University's NSF Engineering Research Center for Plasma-Aided Manufacturing as well as the past chairman of the Department of Electrical and Computer Engineering.

Dr. Shohet is a Fellow of the American Physical Society. He received the Frederick Emmons Terman award of the American Society for Engineering Education, the Merit Award of the IEEE Nuclear and Plasma Sciences Society, the IEEE Richard F. Shea Award, the IEEE Plasma Science Prize, the IEEE Centennial Medal, and the John Yarwood Memorial Medal from the British Vacuum Council. Dr. Shohet founded the IEEE TRANSACTIONS ON PLASMA SCIENCE in 1973.